



Enhancing mechanical properties of polyvinyl alcohol films through cellulose nanocrystals derived from corncob

Getahun Esubalew Demewoz¹ · Asnake Helia Tiruneh¹ · Vincent Herald Wilson² · Swaminathan Jose² · Venkatesa Prabhu Sundramurthy^{3,4}

Received: 21 June 2024 / Revised: 31 August 2024 / Accepted: 4 September 2024
© The Author(s), under exclusive licence to Springer-Verlag GmbH Germany, part of Springer Nature 2024

Abstract

The present study aimed to investigate the influence of incorporating cellulose nanocrystals in a polyvinyl alcohol (PVA) matrix to achieve the enhanced mechanical properties. Cellulose nanocrystals (CNC) were extracted from waste corncob through sulfuric acid hydrolysis. The maximized yield of CNC (41.8%) was observed at the parameters, 65 mass %, 45 °C, and 60 min for sulfuric acid concentration, reaction temperature, and hydrolysis time, respectively. FTIR showed that CNC had evidence with various functional groups. SEM morphology showed that the prepared CNC had needle-shaped and an average length of 170.3 nm. The crystallinity index characterized by XRD for CNCs (79.3%) was found to be higher than the extracted cellulose (76.4%). In addition, the thermal stability using TGA analysis showed that the degradation temperature of the CNC reached around 327 °C, which was higher than that of the raw corncob and extracted corncob cellulose. Further, an investigation was performed on PVA/CNC nanocomposite films that were prepared by solution casting technique using different loadings of resultant CNC (2, 4, and 6 mass%) as nanofillers. By doing so, the tensile strength, elongation, and elastic modulus of polyvinyl alcohol films incorporated with CNC nanofillers were found to be improved significantly.

Keywords PVA · Corncob · Nanocomposites · Cellulose nanocrystal · Tensile strength

1 Introduction

Ecofriendly bio-composites have a tremendous potential to perform as futuristic novel products that could address for remediation of several environmental issues. In this context, an expanding array of applications of cellulose nanocrystals (CNC) in bio-composite preparation gains recent interest as an emerging alternative to other polymeric composites [1]. Accordingly, engineered bio-composites reinforced

with CNC are currently being developed to address diverse demands for eco-friendly and economical commodity products with high performance and durability characteristics toward sustainable prominence [2]. In this line, lignocellulose materials are the most abundant biomass found in almost all the plant-derived materials, particularly, from agricultural residues and municipal solid wastes that can be used as resources for cellulose [3]. As one of the predominate agro-industrial residues, corncob is found to be an abundant agro-residue worldwide that could be exploited for multitudinous applications including cellulose extraction. In general, corncob has a chemical composition of 45% cellulose, 35% hemicellulose, and 15% lignin with other minor components. Chemically purified cellulose derived from corncob is a homo-polysaccharide composed with β -1–4 glucopyranose unit, showing semi-crystalline behavior. It is insoluble in water and common organic solvents, however, extensively used as a cellulose suspension solution in water. Attractively, the characteristics attributes of cellulose, such as low density, favorable mechanical properties, biodegradability, and availability from renewable resources, have

✉ Getahun Esubalew Demewoz
getahune52@gmail.com

¹ Department of Chemical Engineering, Debre Berhan University, Debre Berhan, Ethiopia

² School of Mechanical Engineering, Vellore Institute of Technology, Vellore, India

³ Centre for Natural Products and Functional Foods, Karpagam Academy of Higher Education, Coimbatore, Tamil Nadu, India 641 021

⁴ Department of Biotechnology, Faculty of Engineering, Karpagam Academy of Higher Education, Coimbatore, Tamil Nadu, India 641 021

become remarkable to contribute a rising concerns for this material [4].

Thus far, many researchers have investigated the reinforcement of polymer with nanocellulose materials by virtue of their specific properties related to their lower density, renewability, high strength, biodegradability, transparency, and other properties that cannot be seen in other materials. Among the polymers, polyvinyl alcohol (PVA) has been widely used in research studies for the preparation of blends and composites like chitosan, nitrocellulose, starch, or lignocellulosic fillers [5]. PVA is a recognized synthetic polymer that is favorable to biological systems. Its attributes, including being water-soluble, semi-crystalline, completely biodegradable, non-toxic, and biocompatible, as well as having great optical clarity, make it useful in a wide range of biomedical applications [6]. It is anticipated that the partially hydrolyzed PVA's hydroxyl groups will engage with the CNC's hydrophilic surfaces to form strong hydrogen bonds [7]. Moreover, the biodegradability of PVA enables the production of green nanocomposites when cellulosic materials are incorporated as fillers. Keeping this in view, in this study, amelioration of desirable mechanical properties of PVA by incorporation of highly reactive CNCs isolated from corncobs was examined. Accordingly, designing the hybrid polymer of nanocomposite by thermally-induced phase separation (freeze drying) process and evaluating the material aspects of CNCs/PVA composites has been carried out.

2 Materials and methods

The chemicals used for the study were sulfuric acid (H_2SO_4 , 98%), sodium hydroxide (NaOH, 97%), sodium chlorite (NaClO_2 , 80%), distilled water, toluene (99%), ethanol (97%), glycerol, polyvinyl alcohol (PVA) powder (CH_2CHOH), glacial acetic acid (99.5%), chloroform (99%), and hydrogen peroxide (H_2O_2) were purchased from Alkane PLC, Addis Ababa. All the chemicals used in experiments were of analytical grade and used without further purification.

2.1 Sample collection and preparation

The corncobs were collected from a local field in west Gojjam, Ethiopia. They were washed with deionized water to remove unwanted particles, like dust, and aerosol parts. Then, the washed corncobs were dried in an oven dryer at the temperature of 50 °C for 24 h; further, they were milled with a blender to pass through a 35-mesh screen. After that, the obtained powder having a particle size of less than 150 μm was kept safe in a plastic (polyethylene) bag and stored in a desiccator until use [8]. Then sample was dewaxed in a

Soxhlet apparatus using a mixture of toluene (400 mL) and ethanol (200 mL) solvents with a ratio of 2:1 (v/v) for 6 h at a temperature of 70 °C in a water bath to remove wax, phenolic pigments, and oils. Further, the powder was washed with distilled water. Subsequently, the dewaxed powder was dried in an oven at 50 °C for 24 h to determine the number of extractives and to prepare for the next steps. Here, no color change occurs between the waxed powder and the corncob powder [9].

2.2 Extraction of cellulose

The cellulose extraction from corncobs which consists of breaking up the cobs as a primary step, followed by the non-cellulosic components in corncobs, was removed to isolate cellulose by incorporating procedures documented by Lu and Hsieh [10]. Owing to remove extractives and impurities, it required the following pretreatments to isolate its cellulosic component before acid hydrolysis.

In this respect, dewaxing and alkali bleaching treatments are usually implemented for removing hemicellulose and lignin. Then, during acid hydrolysis, amorphous domains of cellulose are preferentially hydrolyzed, because crystalline regions have a higher resistance to acid attack [11]. The dewaxed corncob (40 g) was treated with a sodium hydroxide aqueous solution of 4% (w/w) at the liquid-to-solid mass ratio of 20:1 for 2 h at 80 °C temperature and 500 rpm under mechanical stirring [8]. It was done to remove lignin and hemicellulose from corncob and to purify the cellulose [12]. Then, the alkaline-treated suspension was vacuum-filtered and washed several times with distilled water until the alkali was completely removed. The alkali treatment was repeated four times and dried at 50 °C for 24 h in an air-circulating oven, followed by a bleaching process which was undertaken for whitening the color [13]. After alkaline treatment, the dried sample was bleached with a solution made up of equal parts (v:v) of acetate buffer (27 g NaOH and 75 mL glacial acetic acid (CH_3COOH), diluted to 1 L of distilled water) and aqueous sodium chlorite (1.7 wt.% NaClO_2 in water). Herein, the ratio of powder to liquid was 1:20 (g/mL) [11]. For bleaching, 40 g of an alkaline-treated cellulose powder sample with powder to liquid ratio of 1:20 (g/mL) was employed. During this step, the solution was treated at 70 °C for 4 h in a water bath under continuous mechanical stirring at an agitation speed of 600 rpm to single out lignin and any organic residues. The suspension was vacuum-filtered, and the solid was repeatedly washed with distilled water until the yellow color disappeared [11]. After ensuring the pH of the fibers became neutral, the resultant samples subsequently dried at 50 °C for 12 h in an air-circulating oven [14]. This procedure was repeated three times using the same conditions followed by the material, corncob cellulose, as resulted. The corncob cellulose was sealed in a

plastic (polyethylene) bag for characterization purposes, and the others are used for acid hydrolysis to prepare cellulose nanocrystals.

2.3 Preparation of cellulose nanocrystals

The corncob cellulose was milled and sieved before hydrolysis and used for the extraction of nanocrystals by acid hydrolysis. In the acid hydrolysis, the diffusion of acid into the amorphous regions and subsequent cleavage of glycosidic bonds took place [15]. The three most important factors, reaction temperature (°C), reaction time (min), and acid concentration (wt.%), were selected for optimizing the acid hydrolysis. The mixture was stirred mechanically continuously until the hydrolysis was completed [16].

After complete hydrolysis of amorphous cellulose, the suspension was diluted with distilled water made up ten times its volume (1500 mL) to the reaction mixture just after termination time to quench the hydrolysis reaction. Then, the diluted suspensions were cooled to room temperature. The suspension was transferred to a 15 mL centrifuge tube followed by centrifuging at 6000 rpm for 15 min to remove excess sulfuric acids [17].

The cellulose nanocrystal was rewashed with distilled water and re-centrifuged three times until the pH value of the suspension reaches above five [18]. Further, the suspension was collected and again diluted with distilled water. The removal of remaining acid, non-reactive salts, and soluble sugars was undertaken by neutralizing the raw product to dialyze against distilled water using a cellulose membrane for 4 days. The suspension of CNCs was sonicated at 25 kHz for 15 min using an ultrasonication instrument [8] to get aqueous homogenized dispersion and labeled as the CNCs suspension. Herein, a few drops of chloroform were added to the freshly prepared suspension to prevent degradation of the cellulose nanocrystals and stored in a refrigerator at 4 °C for characterization. The dimension, surface morphology, crystallinity index, and thermal stability were measured to determine the relationship between the manufacturing process conditions and the resulting properties [18].

2.4 PVA/CNC nanocomposite film preparation

Solvent casting was used to make the CNC/PVA composite films. The PVA powder was mixed with distilled water with a ratio of 1:10. The powder was slowly added to the cold water to avoid the formation of lumps, as it became sticky and the tendency to form lumps increases as temperature rises. The desired amount of glycerol concentration was added and stirred vigorously for 1 h until a homogeneous solution was obtained. To this solution, 30% glycerol was added as a plasticizer to avoid sticking the film to the Petri dish during drying. The mixture was transferred to a

water bath heated to 70 °C and mixed by mechanical agitation for 2 h till the polymer had completely dissolved and a clear jelly-like solution was obtained. Further, the solution was sonicated for 10 min for homogenization [19].

Then, the CNC suspension was slowly added into the stirred PVA solution in a dropwise manner once the polymer fully dissolved. The mixing continued for another hour, followed by a 15-min sonication. The solution was transferred to Petri dishes and kept at 35 °C for 24 h to form nanocomposite film by casting. In order to study the effect of varying nanocellulose amounts on the composite, four sets of nanocellulose suspension were considered. In this regard, various amounts of CNC suspensions (2%, 4%, and 6% by mass) were added to the PVA solution under constant manual stirring until the solution became viscous. The ultrasonication operation was then performed for 15 min in water using a sonicator to obtain a homogeneous mixture and avoid nanocellulose agglomeration in the PVA matrix. Then, the solutions were kept for 24 h to obtain bubble-free solutions before casting on the Petri dish. Different films were cast on the Petri dish according to their perspective ratio and left for 7 days to obtain dry films.

The cooled mixture was poured into petri dishes and the water was allowed to evaporate under laminar air flow at room temperature for 2 days. Films were cast into a petri dish plate with controlled leveling to get uniform thickness. The films were heat-treated in an oven at 50 °C for 3 days. The dried films were carefully peeled from the plates and cut to a specified size. They were stored in desiccators for 5 days at 0–51% RH for each test. The films were de-molded and stored in an environmentally controlled room at 23 °C with the required RH for 2 days before being undertaken for examination.

2.5 Yield of cellulose nanocrystals

The yield of cellulose nanocrystals depends on the parameters, temperature, hydrolysis time, and acid concentration. The acid hydrolysis was able to hydrolyze the cellulose chains to separate the crystalline part from the amorphous part, and it was used to remove the amorphous regions of the cellulose and release cellulose nanocrystals from the cellulose substrate. The yield of cellulose nanocrystals has been determined from Eq. (1).

$$\text{Yield (\%)} = \frac{W_1}{W_2} \times 100 \quad (1)$$

where W_1 represents the dried mass of CNCs obtained after hydrolysis, and W_2 represents the dried mass of cellulose obtained before hydrolysis.

2.6 Physicochemical and molecular characterization

2.6.1 Scanning electron microscopy (SEM)

Scanning electron microscopy (FEI-INSPECT-F50) was performed to observe the morphology and surface structure by scanning the ruptured surface of corncob, alkali-treated corncob, corncob cellulose, and cellulose nanocrystals. It was used to study the effects of various treatments like alkali treatment of sodium hydroxide (NaOH), and bleaching (NaClO₂) on the morphology of the samples [20]. The influence of the alkali treatment of sodium hydroxide (NaOH) and bleaching (NaClO₂) was evaluated through surface morphology and structure of the cellulose nanocrystals. The operation principle for SEM to cross-sectional morphology of the sample was done under vacuum at an accelerating voltage of 2 kV and 8984 magnification [16].

The SEM micrographs provide helpful information about the distribution pattern of the reinforced nanocellulose phase in the PVA matrix such as the morphology of the dispersed polymer matrix, homogenous dispersion, and tendency of agglomeration [21]. It also reveals the bonding network between the PVA matrix and the nanocellulose and whether a rigid percolation-reinforced network was formed or not. In order to determine the morphology and uniform dispersion of nanocellulose in the PVA matrix, the SEM measurement was conducted on PVA/nanocellulose composite film of 6 mass % CNC loading. The morphology of the PVA with 6% CNC composite film was analyzed with the standard procedure of morphology [22].

2.6.2 Particle size determination

The dynamic light scattering (DLS) technique (Malvern, Zetasizer Nano ZS, US) was employed to measure the size of corncob cellulose and cellulose nanocrystal [23]. Malvern Zeta sizer nano (ZE3600) was used to measure particle size, zeta potential, and molecular weight of cellulose nanocrystals. According to ASTM E2834-12 (2018), standard guide for measurement of the particle size distribution of nanomaterials in suspension by nanoparticle tracking analysis (NTA) was carried out [24]. For this purpose, the cellulose nanocrystal suspension was diluted with distilled water, and the measurement was conducted at 25 °C with a calibration time of 80 s. Three measurements were recorded, and the average value was considered.

2.6.3 Fourier transform infrared spectroscopy (FTIR)

Fourier transform infrared spectroscopy (Thermo SCIENTIFIC iS50 ABX) was used to investigate changes that occur in the chemical structure of raw corncob after chemical

treatments (alkaline, bleaching) and acid hydrolysis. The change of the functional groups of raw corncobs, alkali-treated corncob, corncob cellulose, and cellulose nanocrystals (CNCs) was investigated using Fourier transform infrared spectroscopy (FTIR) equipped with KBr beam splitter. This technique was used to identify the changes in the functional group in samples induced by various treatments as a result of chemical modification [20], where the spectra are performed at room temperature in the range of 500 to 4000 cm⁻¹ with the resolution of 4 cm⁻¹.

2.6.4 X-ray diffraction (XRD)

X-ray diffraction (BTX-528) was used to study the crystalline structure of Corncob, alkali-treated corncob, corncob cellulose, and cellulose nanocrystals (CNCs). Here, the operating system (measurement Condition) was set at the voltage of 30 kV and current of 40 mA by applying the irradiation of Cu Kalfa (1.54), at room temperature using a sampling pitch of 0.0200 (°) and preset time 0.40 (s) within a 2θ ranging from 10 to 60° and a scan rate of 3 ° min⁻¹ in continuous scan mode [25]. The crystallinity index (CrI) denotes the ratio of the crystalline constituents to the amorphous regions of the material and is calculated using Eq. (2).

$$\text{CrI} = \frac{I_{200} - I_{\text{am}}}{I_{200}} \quad (2)$$

where I_{200} is the peak intensity, and I_{am} is the minimum intensity.

The coherent volume of the material for each diffraction peak in the crystal often correlates with the size of the crystallite. Occasionally, it also relates to the bulk material's or polycrystalline thin film's thickness, or to the size of the grains in a sample of powder [7].

The Scherrer's equation is used for the determination of the size of particles of crystals in the form of powder, which can be represented in Eq. (3).

$$d = \frac{k\lambda}{\beta \cos\theta} \quad (3)$$

in which, d is the mean size of the ordered (crystalline) domains, k is a shape factor constant value of 0.9, β represents full-width half maximum of maximum (FWHM) intensity in radians, λ is constant radiation with the value of 0.1574 nm, and θ is the Bragg's angle (°).

2.6.5 Analysis of solid-state ¹³C NMR and X-ray photoelectron spectroscopy (XPS)

The ¹³C MAS NMR spectrum was obtained using a solid-state NMR spectrometer (Bruker, HRMAS, Germany) operated at a 75.4 MHz frequency for ¹³C. A frequency

of 300.0 MHz was set for ^1H . For all experiments, a broadband/ ^1H dual frequency 4-mm angle spinning probe head was utilized. The spectra were acquired at a spinning speed and a temperature of 2.000 ± 0.002 kHz and 30°C , respectively. X-ray photoelectron spectroscopy (XPS) technique was executed for the elemental that was determined using an X-ray photoelectron spectrometer [26]. A sample of freeze-dried extracted CNCs sample was analyzed for C1s and O1s spectra by collecting at pass energy of 20 eV with a scan step of 0.1 eV.

2.7 Characterization of CNC/PVA nanocomposite film

2.7.1 Water absorption test

The water absorption behavior of the composite films was evaluated by immersing them in distilled water. For the absorption test, the CNC/PVA composite film was dried in an oven at 50°C for 24 h. Then, the films were cooled in a desiccator, and the weight of each film was taken immediately. The known weights (W_0) of the initial films were fully immersed in distilled water at room temperature for 1 min. The films were taken out of the immersion, and the excess water on the surface of the films was removed by using filter paper, and then the final weight (W_f) was measured and recorded [27]. The percentage of water absorption was calculated for each sample from the increase in initial weight using the following formulas:

$$\text{Water absorption (\%)} = \frac{W_f - w_0}{w_0} \quad (4)$$

where w_0 represents the weight of samples after oven-dry, and w_f represents the weight of samples after exposed to distilled water.

2.7.2 Mechanical properties of CNC/PVA nanocomposites

The effectiveness of reinforcing nanocellulose in the PVA matrix was evaluated in terms of improvement in mechanical properties. High surface area, aspect ratio, high tensile strength, and Young's modulus of nanocellulose are dedicated to improving the mechanical properties of the matrix and the effectiveness of reinforcing ability. The mechanical properties of nanocomposites were studied from the interaction between CNC and PVA matrix. These improvements in mechanical properties such as tensile strength and elongation at break can be obtained from mechanical tests in relation to reinforcement. CNC/PVA composite films were used as material for the mechanical tests. Tensile strength testing, thickness gauge, cutting machine, and steel die of standard dimension equipment were used.

2.7.3 Tensile strength

In order to determine the ultimate tensile strength of the composites, the maximum continuously applied load is divided by the cross-sectional area of the film. The tensile stress may be calculated for any unidirectionally applied load by the following equation.

$$\delta = \frac{P}{tw} \quad (5)$$

where δ , tensile stress; P , applied load; t , average thickness of the film; w , width of the test specimen.

2.7.4 Percent elongation at break (%)

Percent elongation at break is the maximum displacement of the samples at breaks or rupture points multiplied by 100. It can be obtained by dividing the difference between the initial and final specimen length by the initial grip separation length and multiplying the result by a hundred. Percent elongation at the break point was calculated by the following equation.

$$\text{Percentage elongation at break (\%)} = \frac{L_F - L_i}{L_i} \quad (6)$$

where L_F , length at breaking point, and L_i , initial length.

2.7.5 Modulus of elasticity

Young's modulus is obtained by drawing a tangent to the initial linear portion of the load extension curve, selecting any point on this tangent, and dividing the tensile stress by the corresponding strain. It is the slope of the stress-strain curve at the elastic limit region and can be calculated using the following equation.

$$E = \frac{\Delta\delta}{\Delta\epsilon} \quad (7)$$

where E , Young's modulus; $\Delta\delta$, stress difference of two selected; $\Delta\epsilon$, strain difference between two selected points.

2.8 Thermogravimetric analysis (TGA)

The thermal stability of raw corncob, alkali-treated corncob, corncob cellulose, and cellulose nanocrystals was determined by thermogravimetric analysis using a thermogravimetric analyzer [28]. In this present study, the range of temperature for DTG and TGA was set as 30 and 100°C , respectively. Using aluminum pans, a nitrogen environment with a flow rate of 30 mL min^{-1} and a sampling cycle 1500

with a heating rate of $20\text{ }^{\circ}\text{C min}^{-1}$ and a temperature range of 25 to $600\text{ }^{\circ}\text{C}$, sample mass between 5 and 7 mg, were set as the analysis conditions for the TGA Q500 [10].

3 Results and discussion

3.1 Yield of cellulose nanocrystals

The maximum yield of cellulose nanocrystal from corncobs (41.8%) was obtained at the interaction parameters of temperature of $45\text{ }^{\circ}\text{C}$, hydrolysis time of 60 min, and acid concentration of 65 wt.%. Under this condition of parameter interaction, the predicted yield of CNC by using experimental design was obtained at 41.50%. These values were consistent with the literature data [29]. The reduced yield of cellulose nanocrystals by using high concentrations of acid may be related to the hydrolysis process in which cellulose can be degraded to its constituent glucose. Acid hydrolysis hydrolyzed the cellulose chains to separate the crystalline portion from the amorphous portion [13].

3.2 Surface morphology of cellulose nanocrystals and CNC/PVA nanocomposite

In order to understand the surface morphology, the SEM micrograph for CNCs and for PVA/6% CNC composite film morphology of the nanocellulose/PVA was examined. Figure S1(a) shows the scanning electron microscopy images of cellulose nanocrystals after the corncob cellulose was hydrolyzed by sulfuric acid treatment. The rod shape of cellulose nanocrystal resulted due to sulfuric acid and hydrolysis time being so high, which affected the crystalline part of cellulose after destroying the amorphous region [9]. The features of the CNC showed that there was a reduction in the fibrillar structure size and intermittent breakdown in the fibrillar structure into individualizing fibrils. These outcomes were aligned with the findings of Zhang et al. [24]. The results of the morphological investigation by SEM were consistent with other reports in the literature, where CNCs were extracted from different sources [10].

The uniform distribution of cellulose nanocrystals within the host matrix is shown by SEM analysis (Figure S1b). For the PVA/6% CNC composite film analyzed by SEM, the distribution pattern of the nanocellulose in the continuous phase PVA matrix showed uniform distribution. As can be seen from Figure S1, the nanocellulose was uniformly distributed in the PVA matrix, but there were some white-dotted structures observed over the surface of the composite. These white dots could possibly arise from bubbles generated during PVA nanocomposite film production. During the mixing process of PVA with nanocellulose suspension and casting on a Petri dish,

bubbles were generated. During homogenization with ultrasonication, some bubbles were left in the solution and appeared on the film during the casting process which affect the morphology and mechanical properties of the composite. Also, these white dots could be generated during SEM analysis that can possibly form surface charging of the film. The results of the morphological investigation by SEM were consistent with other reports in the literature, where PVA/6% CNC composite film was extracted from different sources [1].

3.3 Particle size analysis

The measurement was conducted at room temperature, and the particle size distribution of cellulose nanocrystals was analyzed from dynamic light scattering (DLS) technique [30]. Table 1 presents the observation from particle size analysis of cellulose nanocrystals in terms of intensity. Figure S2 depicts the intensity of particle size distribution of CNC particles which resulted under the condition of the optimized yield at a desirable parameter interaction of acid concentration and reaction time, and the temperature was an average particle size (diameter) of 170.3 nm at a measurement position of 0.85 mm and a count rate of 9.4 (kcps). This average particle size was a good result; showing the extraction of CNCs from corncob is possible since cellulose nanocrystals have a length in the range of 100–1000 nm and a width between 2 and 15 nm [11] depending on the cellulose source and the chemical treatment applied. Compared to corncob cellulose particle size (1963 nm), the particle size of CNC (170.3 nm) was much smaller; this was because the average particle size (diameter) of CNC depends on hydrolysis parameters that affect the yield.

According to size distribution by intensity data, CNC particles smaller than 170.3 nm were responsible for 100% of the intensity with 24.63 standard deviations.

As shown in Table 2 and Figure S3, size distribution by volume for cellulose nanocrystals has one peak 125.4 nm (diameter) size that is accountable for 100% of volume, and the CNC particles have an average diameter of 170.3 nm with a standard deviation (249.9 nm) diameter.

Table 1 Particle size of cellulose nanocrystals by intensity

			Size (d. nm):	% intensity:	Standard dev (d. nm)
Z-average (d.nm)	170.3	Peak 1:	119.5	100.0	24.63
PdI	0.552	Peak 2:	0.000	0.0	0.000
Intercept	0.823	Peak 3:	0.000	0.0	0.000
Result quality	Good				

Table 2 Particle size of CNC in terms of volume

	Size (d.nm):	% volume:	Standard dev (d.nm)	
Z-average(d.nm)	170.3	Peak 1: 125.4	100.0	249.9
PdI	0.552	Peak 2: 0.000	0.0	0.000
Intercept	0.823	Peak 3: 0.000	0.0	0.000
Result quality	Good			

3.4 FTIR analysis

The functional groups found in raw corncob, alkaline-treated corncob, corncob cellulose, and CNCs were investigated using FTIR spectroscopy.

Figure 1 presents the FTIR spectrum of corncob cellulose, raw corncob, corncob treated with alkali, and the resulting CNC. Table 3 provides the FTIR results and corresponding functional groups present in the samples. Herein, broad bands at 3405 and 3436 cm^{-1} were seen in the samples of raw corncob and alkaline-treated corncob, respectively, as shown in Fig. 1. These peaks are connected to the hydrogen bond O–H stretching vibration, indicating the fiber’s hydrophilic inclination [12]. The peak was observed only

Fig. 1 FTIR spectra of (A) raw corncob, (B) alkali-treated corncob, (C) corncob cellulose, and (D) CNC

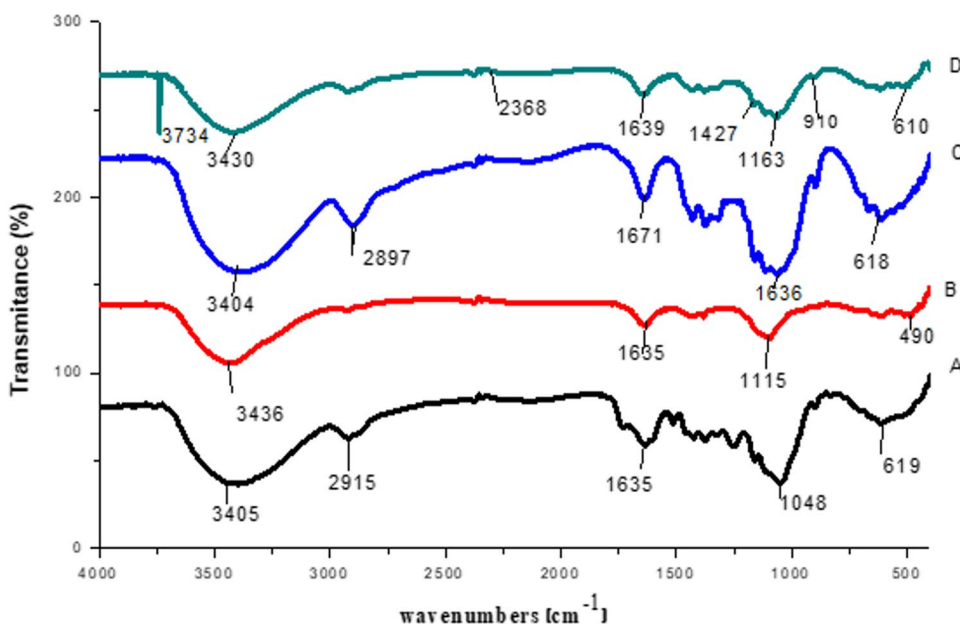
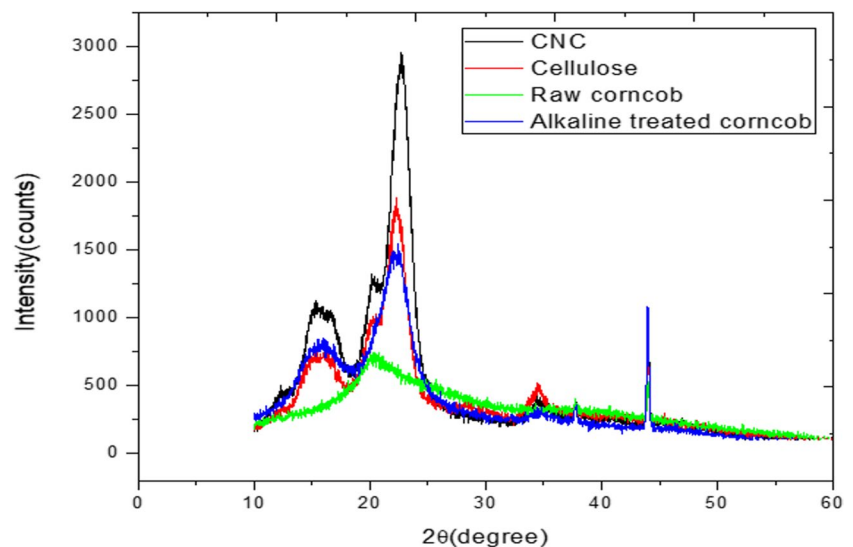


Table 3 The FTIR results and corresponding functional groups are present in the samples

Material/functional group	Peak values							
Raw corncob	610	910	1163	1427	1639	2368	3430	3734
Functional group	C–Br stretch (alkyl halides)	O–H bend Carboxylic acids	C–H wag (–CH ₂ X) Alkyl halides	C–C stretch (in–ring) Aromatics	N–H bend Primary amines	O=C=O stretching	O–H stretch, alcohols	water OH Stretch
Alkali-treated corncob	618	1636	1671	2897	3404			
Functional group	C–Br stretch (alkyl halides)	C=C alkene	C=O amide	–C–H stretch	N–H stretch			
Corncob cellulose	490	1115	1635	3436				
Functional group	Negligible region	C–F	N–H bend Primary amines	O–H stretch, alcohols				
CNC	619	1048	1635	2915	3405			
Functional group	C–Br stretch (alkyl halides)	C–F	N–H bend Primary amines	–C–H stretch	N–H stretch			

Fig. 2 XRD spectra of alkaline-treated corncob, corncob cellulose, raw corncob, and cellulose nanocrystals



in the spectrum of raw corncob at 2915 cm^{-1} which was in the range.

3.5 XRD, XPS, and ^{13}C NMR analysis

The X-ray diffraction patterns were obtained to determine the crystalline index of the raw corncob, alkali-treated corncob, corncob cellulose, and cellulose nanocrystals. The crystallinity index (CrI) refers to the ratio of the crystalline to the amorphous regions of cellulose [3]. Cellulose has a crystalline structure, unlike hemicellulose and lignin. The cellulose crystallinity is due to the interactions between hydrogen and van der Waals forces between adjacent molecules. X-ray diffraction (Fig. 2) was used to determine if there were changes in material crystallinity after different chemical treatments. This indicates that the content of cellulose and the degree of crystallinity was increased, and the crystallinity of cellulose was affected by chemical treatments [12].

As shown in Fig. 2, since the amorphous portions of the raw corncob were eliminated by alkaline, bleaching, and acid hydrolysis processes, cellulose nanocrystals have a large and sharp peak. All samples had a peak at about $2\theta = 22^\circ$. Table 4 provides the crystallinity index of corncob, alkaline-treated corncob, corncob cellulose, and CNC. For raw corncob, alkaline-treated corncob, corncob cellulose, and cellulose nanocrystals, the crystallinity

index (CrI) determined by Eq. (2) were found to be 57.88, 58, 73, and 80, respectively. When compared to raw corncobs, the alkali-treated sample showed the higher CrI value that can be explained by the chemicals involved in the alkali and bleaching treatments applied throughout the purification process. The cellulose nanocrystals' CrI value was higher than that of corncob cellulose because of the partial removal of the para-crystalline domains during the acid hydrolysis. It was found that the acid treatment caused the cellulose nanocrystals to have narrower, sharper peaks because these nanostructures have greater crystallinity than raw fibers. [5].

After alkali treatments and elimination of hemicellulose and lignin present in raw corncob and following acidic hydrolysis by sulfuric acid, amorphous regions in cellulose structure were removed, and the crystallinity index was enhanced. After acidic hydrolysis, the crystallinity index was increased from 57.88 to 79.31%. The increase in the crystallinity index for the raw corncob was due to the removal of hemicellulose and lignin, which exist in amorphous regions. This value is consistent in studies using acidic hydrolysis, and the crystallinity index was between 64 and 91%; however, in most cases, it was around 70% [31]. The crystallinity degree depends on the source of the raw materials, the purification time of the sample, and hydrolysis conditions [32]. According

Table 4 Crystallinity index of corncob, alkaline-treated corncob, corncob cellulose, and CNC

Samples	2θ (amorphous) ($^\circ$)		2θ (002) ($^\circ$)		CrI (%)
	Degree	Intensity (I_{am})	Degree	Intensity (I_{002})	
Raw corncob	34	310	20.15	736.41	57.88
Alkaline-treated corncob	19.12	603.08	22.31	1536.27	58
Corn-cob cellulose	17.86	445.04	22.42	1887.87	73
CNC	17.86	598.72	22.75	2893.5	80

Fig. 3 XPS spectra of CNC (a) and high-resolution XPS spectra of C1s for CNC (b)

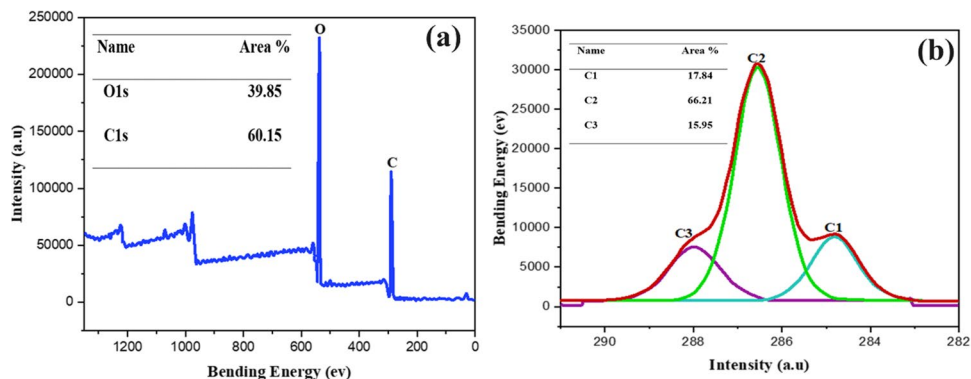


Table 5 Peak data list for cellulose nanocrystals

Peak no	2θ (°)	d(A)	I/II	FWHM (°)	Intensity (counts)	Integrated intensity (counts)
1	12.4843	7.08448	6	1.68000	95	9614
2	15.3938	5.75140	27	2.23200	449	37,127
3	16.5310	5.35822	24	2.14280	399	35,354
4	20.3219	4.36644	33	1.60000	546	52,367
5	22.6665	3.91980	100	2.00700	1662	161,652
6	25.1907	3.53245	4	1.00000	73	8736
7	34.7082	2.58251	6	2.06000	94	10,890
8	37.8021	2.37795	4	0.70670	67	3898
9	44.0081	2.05593	16	0.56400	262	7620
10	64.3689	1.44617	12	0.56140	199	5818
11	77.4730	1.23102	13	0.55070	210	5761

to Fig. 3, Table 5 displays the 11 peaks and the crystallite size for cellulose nanocrystals that were determined using Eq. (3).

As anticipated, in the XPS survey spectrum, two distinct peaks of carbon (about 286 eV) and oxygen (about 532 eV) were found for the CNC sample (Fig. 3). As displayed in

Fig. 4 NMR measurement for a freeze-dried sample of resultant CNC

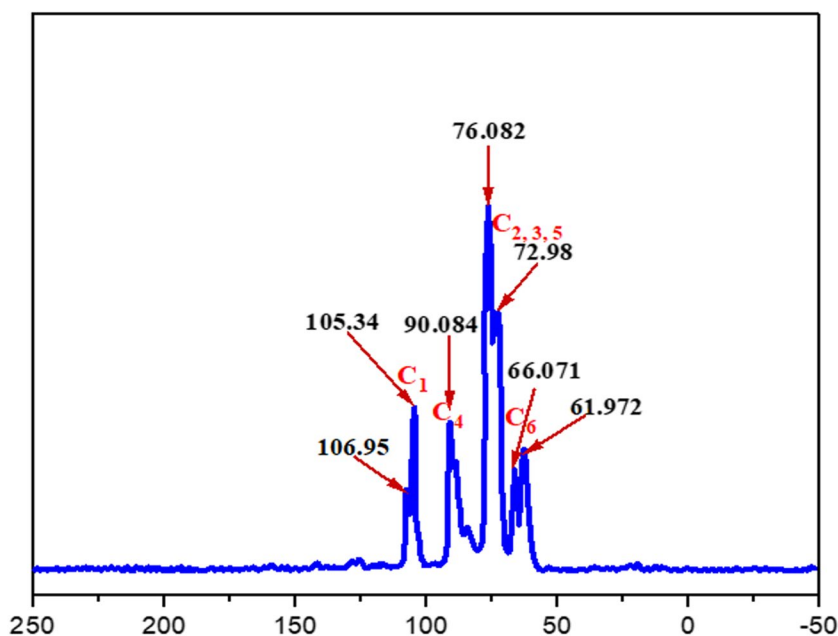


Fig. 5 TGA profiles for the composite films of PVA/0%CNC, PVA/2%CNC, PVA/4%CNC, and PVA/6%CNC

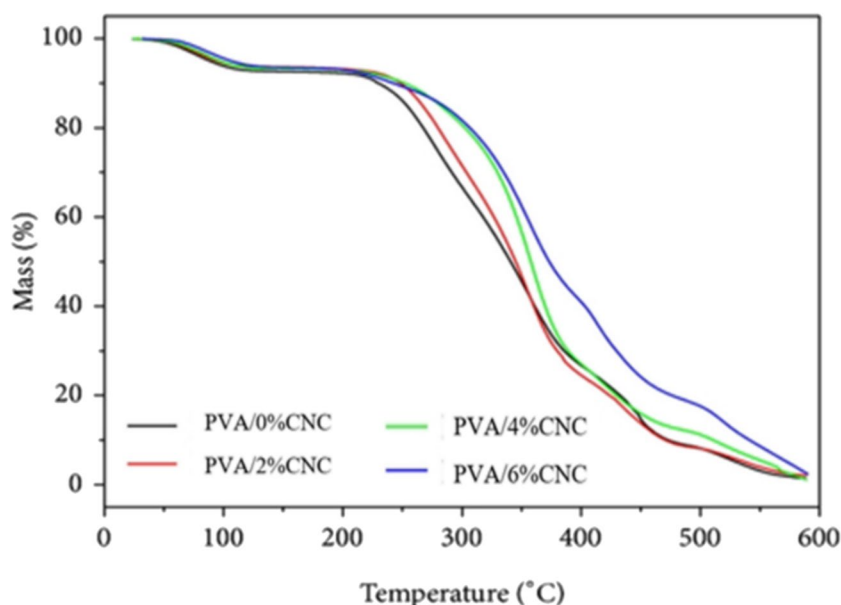


Fig. 3a, the high-resolution carbon spectra of the C1s signals for CNC have been broken down into three different types of component peaks (C1, C–C and C–H; C2, C–O; and C3, C=O and O–C–O). As per the previous documentation, CNC showed three peaks at around 284.8 eV, 286.4 eV, and 288.1 eV, which correspond to C1, C2, and C3. The area of peaks can be used to compute the relative amounts of each C1s component; the findings are displayed in the inset table. The acquired results from NMR measurement for freeze-dried sample of resultant CNC are shown in Fig. 4. It was observed that the CNC sample displayed a standard NMR spectrum. The region between 61.972 and 66.071 ppm can be assigned to C6 which could be categorized as the primary alcohol group. The following resonance peaks, which

were rather large and fell between 75.98 and 76.082 ppm, were ascribed to the ring carbons C2, C3, and C5, which were not connected by the glycosidic bond. The ring carbon, C4 and C1, were represented by the areas between 86 and 107 ppm and the acute resonance at 90.084 and 105.34 ppm, respectively. The outcomes of the XPS measurements were validated by the NMR data.

3.6 Thermal stability analysis

Thermogravimetric analysis (TGA) is an important method for understanding the thermal stability of polymer bio nanocomposites [33, 34]. TGA was used to investigate the thermal degradation behavior of PVA films loaded with different

Fig. 6 DTG curves for films obtained from the composites, PVA/0%CNC, PVA/2%CNC, PVA/4%CNC and PVA/6%CNC

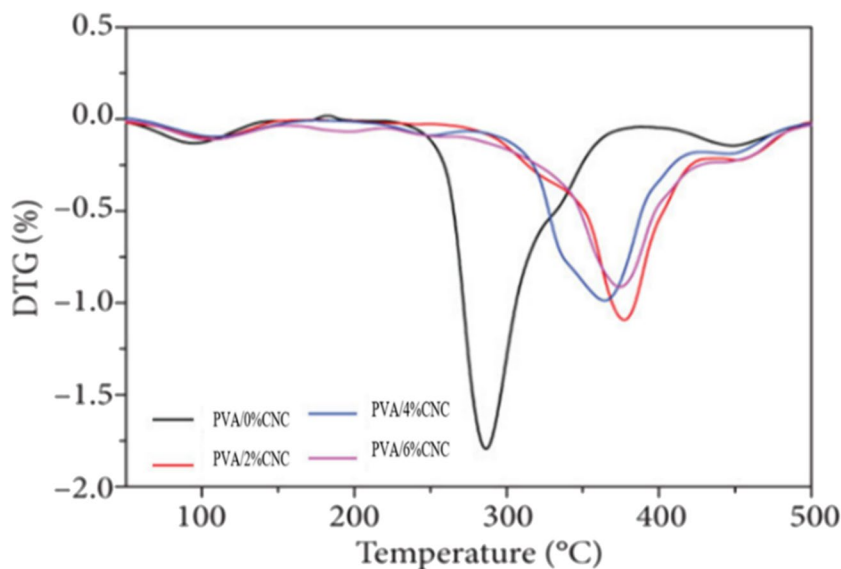


Table 6 Pyrolysis temperature characteristics of composite samples

Composite	Onset temperature (°C)	Offset temperature (°C)	Mass loss (%)	Residual mass (%)
PVA/0%CNC	234.5	284.4	83.42	16.58
PVA/2%CNC	349.4	384.2	77.53	22.47
PVA/4%CNC	333.4	359.7	78.21	21.79
PVA/6%CNC	333.2	359.2	77.26	22.74

Table 7 Water absorption test

Composite	Water absorption capacity
Neat PVA	82.8289 ± 0.56
PVA/2 mass % CNC	48.42324 ± 0.62
PVA/4 mass % CNC	38.43587 ± 0.76
PVA/6 mass % CNC	25.32975 ± 0.82

mass % of CNC. Accordingly, TGA continuously measures the mass of a sample as a function of temperature.

The obtained TGA and DTG curves are shown in Figs. 5 and 6, respectively. Table 6 presents the pyrolysis temperature characteristics of CNC composite samples. The TGA curves for both films showed that three mass loss regions occur in the range of 30 to 180 °C during the first stage of degradation. This is related to the evaporation of absorbed water, 10.86% for pure PVA and 7.4% For PVA composites. The second range was from 200 to 370 °C and is due to degradation of PVA due to degradation of the intermolecular hydrogen bonds of PVA due to dehydration reactions on the polymer chains and degradation of the backbone. The third region is above 400 °C, indicating charring of the organic

material. As can be seen, the DTG curve for the pure PVA film reached the maximum peak at a temperature of 290 °C, while the nanocellulose-enhanced PVA film reached the maximum peak at 275 °C. After tempering, the thermal decomposition temperature of the PVA film shifted to a lower temperature. Residual char was higher in PVA composite films than in pure PVA. This indicated a decrease in the thermal stability of his PVA after incorporating nanocellulose particles. This was due to the lower thermal stability of CNC compared to PVA polymers. Nanocellulose extracted with sulfuric acid is less stable than those extracted by other methods due to the formation of sulfate groups on the nanocellulose during the acid hydrolysis process and the thermal decomposition of the sulfate groups begins at low temperatures.

3.7 Water absorption test result

Table 7 and Fig. 7 below summarize the percentage water absorption capacity of the composites obtained by immersing in distilled water for one minute.

Figure 7 shows that increasing in loading of nanocellulose in the PVA matrix decreases water intake capacity. This could be due to nanocellulose forming rigid network bond that resists water absorption to enter freely into composite molecules. Therefore, as the mass percentage of nanocellulose increases in the PVA matrix, rigidity also increases, resulting in water intake decrease.

3.8 Mechanical properties

The average values of tensile stress, tensile strain, Young’s modulus, and elongations at the break of the prepared films are presented below.

Fig. 7 Comparative study on percentage water absorption between CNC reinforced PVA films and neat PVA films

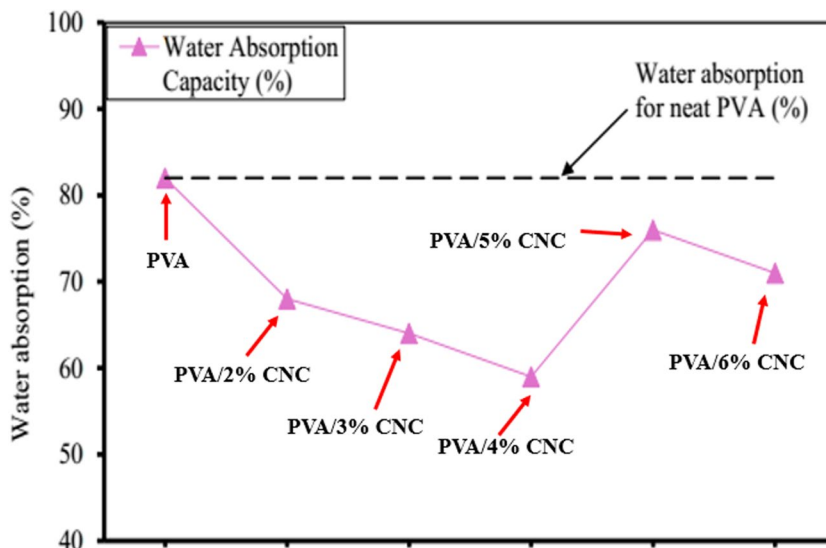


Table 8 Results obtained for tensile strength of different PVA/CNC combinations

Composite	Maximum tensile strength (MPa)
Neat PVA	33.5
PVA/2 mass % CNC	40
PVA/4 mass % CNC	53.34
PVA/6 mass % CNC	37.3

3.8.1 Tensile strength

PVA and CNCs with five different ratios based on mass percentage have been undertaken, and each specimen was used for examination [35]. From load-deformation, the corresponding stress–strain curves of the reinforced PVA nanocomposite films under tensile loading are given in Table 8 and Fig. 8. Engineering stress/strain was obtained by taking the load and deformation of a given specimen as primary output from the experiment that defined the curve of stress–strain.

Table 9 Elongation at break (%) result

Composite	Elongation @break (%)
Neat PVA	358
PVA/2 mass % CNC	192.525
PVA/4 mass % CNC	147
PVA/6 mass % CNC	302

3.8.2 Elongation at break

Percent elongation at break was calculated by dividing the extension at the moment of rupture of each specimen by the initial grip separation of the specimen and multiplying by 100. As shown in Table 9 and Fig. 9, elongations at break were obtained from the average of each five test specimens for all formulations of composites.

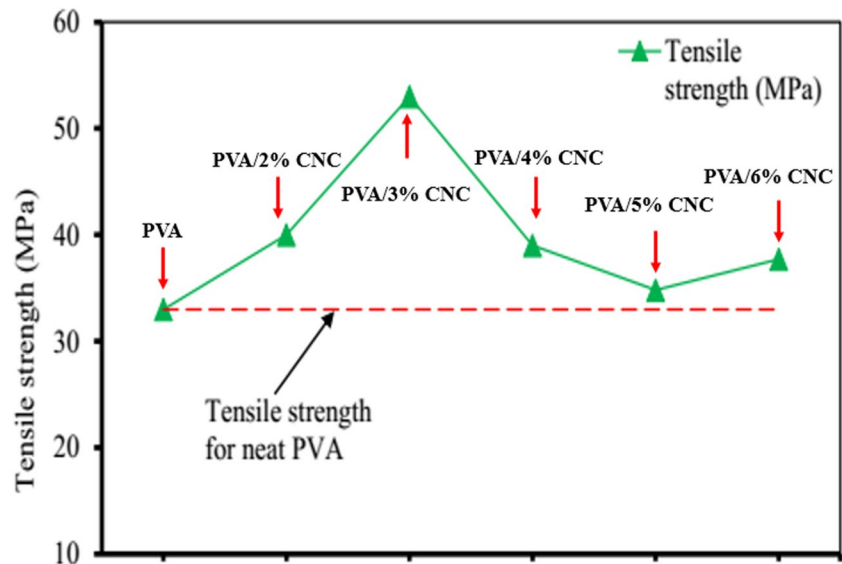
Fig. 8 Comparative study on tensile strength of PVA composite films and tensile strength of neat PVA film

Fig. 9 Comparative study on elongation at break (%) of PVA composite films and elongation at break of neat PVA film

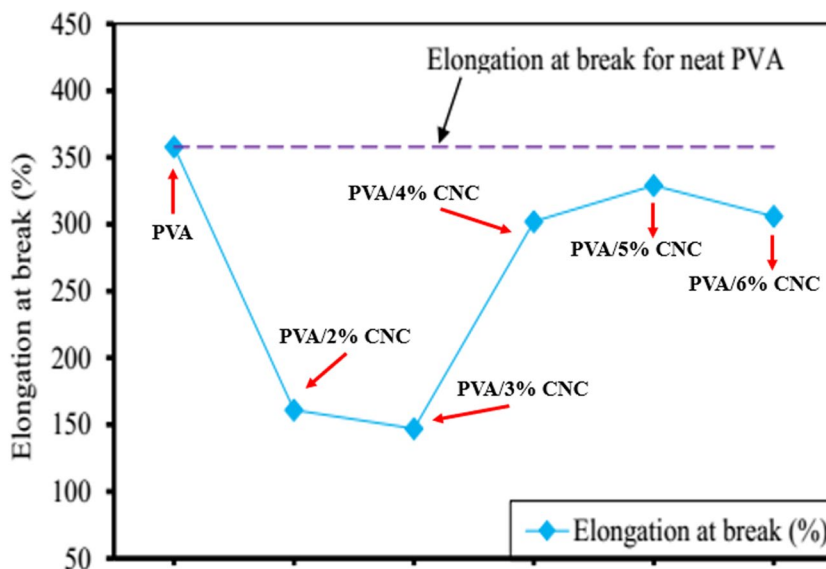


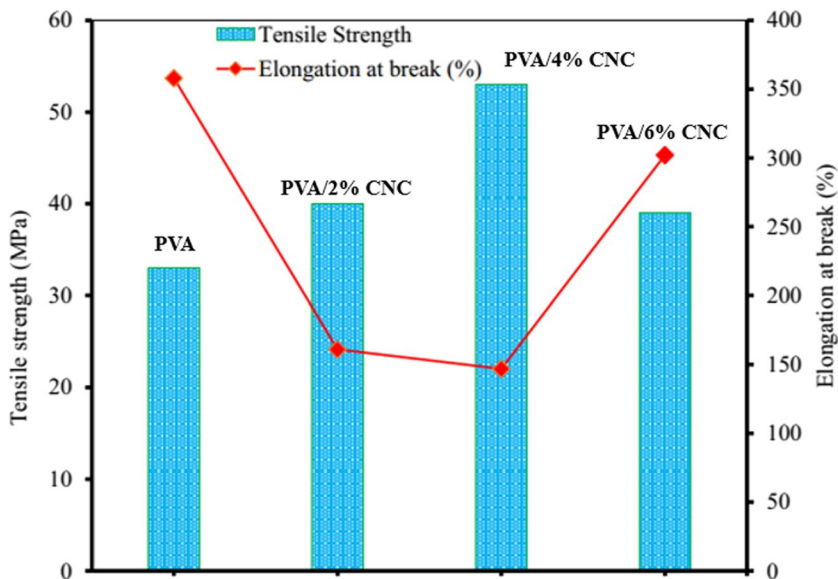
Table 10 Modulus of elasticity of different combinations of PVA/CNC composites

Composite	Young's modulus (GPa)
Neat PVA	0.990
PVA/2 mass % CNC	1.2242
PVA/4 mass % CNC	1.4043
PVA/6 mass % CNC	1.6548

3.8.3 Modulus of elasticity

The Young's modulus is the slope of the linear elastic deformation of the stress-strain curve. It shall be calculated by drawing a tangent to the initial linear portion of the load-extension curve, selecting any point on this tangent, and dividing the tensile stress by the corresponding strain [36]. Table 10 presents the results obtained for the modulus of elasticity value of different combinations of PVA/CNC composites.

Fig. 10 The elongation at break and tensile strength of the PVA/CNC composite films as a function of the CNC content



3.8.4 Comparison of cellulose nanocrystal reinforcement in PVA

The results showed that the increase in the nanocellulose loading in the PVA matrix reduces percent elongation at break for all filler cases. As clearly shown in Fig. 10, neat PVA film has a high percent elongation at break compared to PVA reinforced with nanocellulose filler. For 2% loading of nanocellulose in the matrix, elongation at break was reduced by 32.3%. Similarly, for 2%, 4%, and 6% mass loading, the nanocomposite has shown reduced value of percent elongation 50.5%, 56.7%, and 24.9%, respectively.

4 Conclusion

In this study, the valorization of corncobs with respect to cellulose nanocrystal (CNC) production and its effect on the reinforcement of PVC for preparing bio-nanocomposite films with good thermal and mechanical properties have been investigated. CNCs were successfully extracted from waste corncobs through the sulfuric acid hydrolysis method and characterized by different techniques. Further, CNCs were implemented to reinforce with polyvinyl alcohol by the solvent casting technique. The effect of reinforcement of CNCs in the PVA matrix on its mechanical properties, water intake capacity, thermal stability, and biodegradability was examined. This work implied that the properties of PVA in terms of tensile strength, elongation at break, and water absorption capacity were improved significantly due to good compatibility between the PVA matrix and extracted CNCs. The particle size analyzer revealed that extracted CNCs from corncob had an average length of around 170.3 nm. By adding 6 mass % CNC, there was a 17.9% increment of maximum tensile stress, a 67.15% increase of Young's modulus, and a 56.7% decrement in percent elongation at break. Thermo gravimetric test of the nanocomposite reinforced by 6 mass% CNC showed thermal stability that can withstand up to 500 °C temperature. The study showed that the nanocellulose extracted from the corncob can be a good source to use as a reinforcing agent of the PVA matrix to prepare a futuristic bio-based eco-friendly material.

Supplementary Information The online version contains supplementary material available at <https://doi.org/10.1007/s13399-024-06128-6>.

Acknowledgements The authors express their sincere appreciation to the Debre Berhan University, Debre Berhan, Ethiopia.

Author contribution Getahun Esubalew Demewoz conducted the experiments; Asnake Helia Tiruneh designed and validated formal analysis; S. Venkatesa Prabhu performed correction of context and formatted and corrected the context; Vincent Herald Wilson and Swaminathan Jose conceptualized, wrote, and supervised the whole manuscript.

Data availability Data and materials can be given on request-based.

Declarations

Competing interests The authors declare no competing interests.

References

1. Luzi F, Fortunati E, Jiménez A, Puglia D, Chiralt A, Torre L (2017) PLA nanocomposites reinforced with cellulose nanocrystals from *Posidonia oceanica* and ZnO nanoparticles for packaging application. *J Renew Mater* 5(2):103–115. <https://doi.org/10.7569/JRM.2016.634135>
2. Trache D, Hussin MH, Hui Chuin CT, Sabar S, Fazita MRN, Taiwo OFA, Haafiz MKM (2016) Microcrystalline cellulose: Isolation, characterization and bio-composites application—a review. *Int J Biological Macromol* 93(June2018):789–804
3. Yang ST (2017) Bioprocessing—from biotechnology to biorefinery. *Bioprocessing for Value-Added Products from Renewable Resources* 1–24. <https://doi.org/10.1016/B978-0-44452114-9/50002-5>
4. Akhlamadi G, Goharshadi EK, Liimatainen H (2022) *J Mater Chem A* 10(46):24746–24760. <https://doi.org/10.1039/D2TA06437E>
5. TersurOrasugh J, Dutta S, Das D, Nath J, Pal C, Chattopadhyay D (2019) Utilization of cellulose nanocrystals (CNC) biopolymer nanocomposites in ophthalmic drug delivery system (ODDS). *J Nanotechnol Res* 01(02):75–87. <https://doi.org/10.26502/jnr.2688-8521006>
6. Abitbol T, Rivkin A, Cao Y, Nevo Y, Abraham E, Ben-Shalom T, Shoseyov O (2016) Nanocellulose, a tiny fiber with huge applications. *Current Opin Biotech* 39(October 2017):76–88
7. Jiang Y, Liu L, Yan J, Wu Z (2024) Room-to-low temperature thermo-mechanical behavior and corresponding constitutive model of liquid oxygen compatible epoxy composites. *Compos Sci Technol* 245:110357. <https://doi.org/10.1016/j.compscitech.2023.110357>
8. Huang S, Zhou L, Li MC et al (2017) Cellulose nanocrystals (CNCs) from corn stalk. 1–13. <https://doi.org/10.3390/ma10010080>
9. Akhlamadi G, Goharshadi EK (2021) Sustainable and superhydrophobic cellulose nanocrystal-based aerogel derived from waste tissue paper as a sorbent for efficient oil/water separation. *Process Saf Environ Prot* 154:155–167. <https://doi.org/10.1016/j.psep.2021.08.009>
10. Cen Q, Xing Z, Wang Q, Li L, Wang Z, WuLiu ZL (2024) Molding simulation of airfoil foam sandwich structure and interference optimization of foam-core. *Chin J Aeronaut*. <https://doi.org/10.1016/j.cja.2024.08.025>
11. Patients S, PC in SC, Hassan BAR, Yusoff ZBM, Othman MAH, Bin S, Chapter A (2012) Information is available at the end of the, & <http://dx.doi.org/https://doi.org/10.5772/55358>. (2012). We are IntechOpen, the world's leading publisher of Open Access books Built by scientists, for scientists TOP 1 %. <https://doi.org/10.1016/j.colsurfa.2011.12.014>
12. Thakur M, Sharma A, Ahlawat V, Bhattacharya M, Goswami S (2020) Process optimization for the production of cellulose nanocrystals from rice straw derived a -cellulose. *Mater Sci Energy Technol* 3:328–334. <https://doi.org/10.1016/j.mset.2019.12.005>
13. Larissa LA, Fonsêca AF, Pereira FV, Druzian JI (2015) Extraction and characterization of cellulose nanocrystals from corn stover. *Cellul Chem Technol* 49(2):127–133

14. Flauzino Neto WP, Silvério HA, Dantas NO, Pasquini D (2013) Extraction and characterization of cellulose nanocrystals from agro-industrial residue - soy hulls. *Ind Crops Prod* 42(1):480–488
15. Dan Chen ME (2011) Biocomposites reinforced with cellulose nanocrystals derived from potato peel waste biocomposites reinforced with cellulose nanocrystals derived from potato peel waste. *Carbohydrate Polymers* 90:709
16. Manaf EA, Mohamad N, Sakinah S, Ahmad S (2019) Extraction and characterisation of cellulose nanocrystals structures from waste office paper. 2(2):202–211
17. Wang Y, Xu Y, Zhai W, Zhang Z, Liu Y, ChengZhang SH (2022) In-situ growth of robust superlubricated nano-skin on electrospun nanofibers for post-operative adhesion prevention. *Nat Commun* 13(1):5056. <https://doi.org/10.1038/s41467-022-32804-0>
18. Leite ALMP, Zanon CD, Menegalli FC (2017) Isolation and characterization of cellulose nanofibers from cassava root bagasse and peelings. *Carbohyd Polym* 157:962–970. <https://doi.org/10.1016/j.carbpol.2016.10.048>
19. Orue A, Santamaria-Echart A, Eceiza A, Peña-Rodríguez C, Arbelaiz A (2017) Office waste paper as cellulose nanocrystal source. *J Appl Polym Sci* 134(35):1–11. <https://doi.org/10.1002/app.45257>
20. Akhlamadi G, Goharshadi EK (2021) Siavosh Vojdani Saghir, Extraction of cellulose nanocrystals and fabrication of high alumina refractory bricks using pencil chips as a waste biomass source. *Ceram Int* 47(19):27042–27049. <https://doi.org/10.1016/j.ceramint.2021.06.117>
21. Pereira B, Arantes V (2018) Nanocelluloses from sugarcane biomass. *Advances in sugarcane biorefinery: technologies, commercialization, policy issues and paradigm shift for bioethanol and by-products* (January) 179–196. <https://doi.org/10.1016/B978-0-12-804534-3.00009-4>
22. Singh S, Gaikwad KK, Park S, Lee YS (2017) Microwave-assisted step reduced extraction of seaweed (*Gelidiella acerosa*) cellulose nanocrystals. *Int J Biol Macromol* 99:506–510. <https://doi.org/10.1016/j.ijbiomac.2017.03.004>
23. Kandhola G, Djioleu A, Rajan K, Labbé N, Sakon J, Carrier DJ, Kim JW (2020) Maximizing production of cellulose nanocrystals and nanofibers from pre-extracted loblolly pine kraft pulp: a response surface approach. *Biores Bioprocess*. <https://doi.org/10.1186/s40643-020-00302-0>
24. Zhang PP, Tong DS, Lin CX et al (2014) Effects of acid treatments on bamboo cellulose nanocrystals. (April):686–695. <https://doi.org/10.1002/apj>
25. Henrique MA, Silvério HA, Pires W, Neto F, Pasquini D (2013) Valorization of an agro-industrial waste, mango seed, by the extraction and characterization of its cellulose nanocrystals. *J Environ Manage* 121:202–209. <https://doi.org/10.1016/j.jenvman.2013.02.054>
26. Xie H, Du H, Yang X, Si C (2018) Recent strategies in preparation of cellulose nanocrystals and cellulose nanofibrils derived from raw cellulose materials. *Int J Polym Sci* 2018:25
27. Zhang G, Wu F, Ma T, Zhang B, Manyande A, Du H (2019) Preparation and characterization of cellulose nanofibers isolated from lettuce peel. *Cellul Chem Technol* 53(7–8):677–684
28. Evans SK, Wesley ON, Nathan O, Moloto MJ (2019) Helicon chemically purified cellulose and its nanocrystals from sugarcane baggase: isolation and characterization. *Heliyon* 5(October):e02635. <https://doi.org/10.1016/j.heliyon.2019.e02635>
29. Alves H, Pires W, Neto F, Oliveira N, Pasquini D (2013) Extraction and characterization of cellulose nanocrystals from corncob for application as reinforcing agent in nanocomposites. *Ind Crops Prod* 44:427–436. <https://doi.org/10.1016/j.indcrop.2012.10.014>
30. Zhou YM, Fu SY, Zheng LM, Zhan HY (2012) Effect of nanocellulose isolation techniques on the formation of reinforced poly(vinyl alcohol) nanocomposite films. *Express Polym Lett* 6(10):794–804
31. Hernandez CC, Ferreira FF, Rosa DS (2018) X-ray powder diffraction and other analyses of cellulose nanocrystals obtained from corn straw by chemical treatments. *Carbohyd Polym* 193(January):39–44
32. Hemmati F, Mahdi S, Kashaninejad M, Barani M (2018) Synthesis and characterization of cellulose nanocrystals derived from walnut shell agricultural residues. *Int J Biol Macromol* 120:1216–1224. <https://doi.org/10.1016/j.ijbiomac.2018.09.012>
33. Nyakuma BB, Wong S, Oladokun O (2021) Non-oxidative thermal decomposition of oil palm empty fruit bunch pellets: fuel characterisation, thermogravimetric, kinetic, and thermodynamic analyses. *Biomass Conv Bioref* 11:1273–1292. <https://doi.org/10.1007/s13399-019-00568-1>
34. Oladokun O, Ahmad A, Abdullah TAT (2016) Bemgba Bevan Nyakuma, Aliyu Abdul-Hameed Bello, Ali Hussein Al-Shatri, Multicomponent devolatilization kinetics and thermal conversion of *Imperata cylindrica*. *Appl Therm Eng* 105:931–940. <https://doi.org/10.1016/j.applthermaleng.2016.04.165>
35. Faria M, Thomas S, Pothan LA (2015) Utilization of various lignocellulosic biomass for the production of nanocellulose: a comparative study. 1075–1090. <https://doi.org/10.1007/s10570-015-0554-x>
36. Wang Y, Zhai W, Li J, Liu H, LiLi CJ (2023) Friction behavior of biodegradable electrospun polyester nanofibrous membranes. *Tribol Int* 188:108891. <https://doi.org/10.1016/j.triboint.2023.108891>

Publisher's Note Springer Nature remains neutral with regard to jurisdictional claims in published maps and institutional affiliations.

Springer Nature or its licensor (e.g. a society or other partner) holds exclusive rights to this article under a publishing agreement with the author(s) or other rightsholder(s); author self-archiving of the accepted manuscript version of this article is solely governed by the terms of such publishing agreement and applicable law.